Dalton Transactions

Accepted Manuscript

Volume 1 | Number 1 | Jan 2013 | Pages 1–100

Dalton Transactions

An international journal of inorganic chemistry
www.rsc.org/dalton

ROYAL SOCIETY OF CHEMISTRY

ROYAL SOCIETY OF CHEMISTRY

www.rsc.org/dalton

ARTICLE TYPE

Shaping and Enforcing Coordination Spheres: Probing the ability of Tripodal ligands to Favour Trigonal Prismatic Geometry

James C. Knight, Angelo J. Amoroso,* Peter G. Edwards, Neha Singh and Benjamin D. Ward.

We report two tripodal frameworks, mono(2,2'-bipyrid-6-yl)bis(2-pyridyl)methanol (L^1) and bis(2,2'-bipyrid-6-yl)mono(2-pyridyl)methanol (L^2) which have one and two bipyridyl arms, respectively. Both ligands form complexes with the first row transition metals. Both ligands appear to overcome the steric strain involved in twisting the ligand to produce an octahedral 10 complex and the solid state structures in general show more octahedral character than complexes of the related ligand, tris(2,2'-bipyrid-6-yl)methanol (L^3). Continuous Shape Mapping (CShM) calculations based on crystallographic data reveal that L^1 is incapable of enforcing a trigonal prismatic (TP) co-ordination geometry in the solid state, surprisingly even upon co-ordination to metals with no stereochemical preference such as cadmium (S(TP) = 7.15 and S(Oh) = 3.95). However, ligand L^2 clearly maintains an ability to enforce a trigonal prismatic conformation which is demonstrated in the crystal 15 structures of the Mn^{II} and Cd^{II} complexes (S(TP) = 0.75 and 1.09, respectively). While L^3 maintains near-TP configurations in the presence of metal ions with strong octahedral preferences, L^2 distorts towards predominantly octahedral co-ordination geometries, increasing in the order $Co^{II}<Ni^{II}<Fe^{II}$ and no trigonal prismatic structures.

Introduction

The trigonal prismatic geometry is the rarer form of six co-20 ordinate geometry when contrasted to the almost ubiquitous octahedral alternative. It was not until 1965, when Ibers and Eisenberg[1,2] charactered a rhenium dithiolato complex, that trigonal prismatic geometry was crystallographically characterised in a discrete molecular compound. Soon after, 25 other early transition metal dithiolate complexes that also displayed trigonal prismatic geometries were reported,[3] with the geometric preference being thought to be determined, in part, to S-S inter-ligand bonding,[4] although since then an number of non-thiolate didentate ligands, such as 30 acetylacetone and buta-1,3-diene, have been shown to form trigonal prismatic complexes.[5]

Later, Wentworth reported the synthesis of rigid polydentate ligands with donor atoms fixed in the positions of the vertices of a trigonal prism.[6] With transition metal ions he observed 35 TP geometry for Zn^{II} but significant distortion to Oh geometry with Fe^{II} and Ni^{II}. A Bailar twist angle of 32 ° was later determined for the Ni^{II} complex.[7] The tendency for the late transition metals to distort the complex towards an octahedral geometry was explained by simply considering the difference 40 in ligand field stabilisation energy for the two alternative structures (Figure 1). By this consideration, low spin d^5, d^6 and d^7 as well as d^8 ions should show the greatest tendency towards octahedral geometry, while high spin d^5 and d^6 as well as d^{10} ions have no preference and will form geometries 45 primarily determined by the steric demands of the ligand. Following these tripodal ligands, a series of bimacrocyclic ligands were reported by Rose,[8] Holm[9] and Raymond.[10] Recently, we reported an investigation into the tripodal bipyridine-based ligand tris(2,2'-bipyrid-6-yl) methanol (L^3; 50 Fig. 1) which demonstrated an ability to enforce a

predominantly TP co-ordination geometry upon metal ions with a strong octahedral preference.[11] More recently Alberto reported an alternative synthesis of the analogous tetra[12]- and pentadentate[13] tripodal ligands, mono(2,2'-bipyrid-6-55 yl)bis(pyrid-2-yl)methanol and bis(2,2'-bipyrid-6-yl)mono(pyrid-2-yl)methanol (L^1 and L^2 respectively; Fig. 1) which when co-ordinated to Co^{II} was shown to be an effective water reducing catalyst.
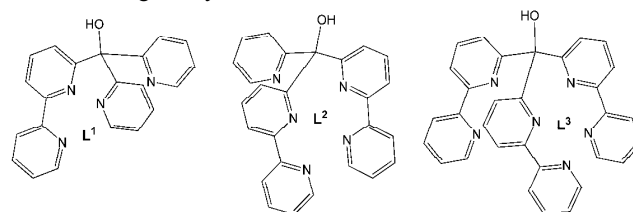
Fig. 1 The tripodal ligands L^1, L^2 and tris(2,2'-bipyrid-6-yl) methanol 60 (L^3). Ligand L^3 is capable of enforcing a trigonal prismatic co-ordination geometry upon metals with a strong octahedral preference.

Since these ligands contain fewer bipyridyl arms than L^3, it is clear that the steric strain involved in twisting the ligand to produce an octahedral geometry is decreased. It may be 65 anticipated that the stereoelectronic preference of the metal ion becomes a more dominant factor in establishing ligand conformation compared to L^3. With this in mind, a quantitative analysis of the co-ordination polyhedral *via* CShM calculations[14] based on crystallographic data has been 70 undertaken to determine each ligands ability to enforce a trigonal prismatic conformation upon metal centres with varying d^n-electron configurations.

Experimental

General

75 NMR spectra were measured on a Bruker AM-400 or Bruker Av-500 Plus FT-NMR spectrometer. For infrared spectra,

each compound was pressed into a disk with an excess of dried KBr and measured on a Jasco FT-IR spectrophotometer. Electrospray (ES) and high-resolution (HR) mass spectra were measured on a Waters LCT Premier XE (oa-TOF) mass spectrometer. UV-VIS absorption spectra were run in HPLC grade acetonitrile (Fisher) and measured on a Jasco V-570 spectrophotometer from 200 to 1,100 nm (optical path length 1.0 cm). Elemental analyses were carried out by the Warwick Analytical Service, University of Warwick.

Preparations

Mono(6-bromopyrid-2-yl)bis(pyrid-2-yl)methanol

2,6-dibromopyridine (1.09 g, 4.6 mmol) was dissolved in diethyl ether (46 mL). With vigorous stirring, the temperature was lowered to -78°C and one molar equivalent of n-BuLi (2.88 mL, 4.6 mmol of a 1.6M solution in hexane) was added dropwise. After stirring for 5 mins, a solution of bis(2-pyridyl)ketone (0.77 g, 4.2 mmol) in THF (14 mL) was slowly transferred to the lithiate. After stirring for a further 24 h at -78°C the reaction was allowed to warm to 0°C and was quenched with 10% aqueous K_2CO_3. The crude product was partitioned between $CHCl_3$ and water. The aqueous layer was washed twice with $CHCl_3$ (60 mL) and the organic layers were combined and dried with anhydrous $MgSO_4$. After filtration, the organic solvent was evaporated under reduced pressure. A dark oily crude product was obtained which was chromatographed on silica gel and eluted with DCM/MeOH (95:5) to give a pale yellow solid (42%). ^1H NMR ($CDCl_3$): δ 6.90 (s, 1H, O*H*), 7.10 (d, 1H, *J* 7.9 Hz), 7.25 (dd, 2H, *J* 6.4, 1.7 Hz), 7.45 (d, 1H, *J* 7.4 Hz), 7.60-7.70 (m, 5H), 8.45 (d, 2H, *J* 6.4 Hz). ^{13}C NMR ($CDCl_3$): δ 79 (C-O*H*), 121, 122, 123, 126, 136,138, 139, 147, 161, 164; IR KBr/cm^{-1}: ν = 3407m, 1595s, 1563m, 1428s, 1410m, 1171m, 1141m, 996s, 804m, 755w, 704m; accurate EIMS (*m/z*): 342.0237 [M + H]$^+$.

Bis(6-bromopyrid-2-yl)mono(pyrid-2-yl)methanol

2-bromopyridine (0.88 mL, 9.2 mmol) was dissolved in diethyl ether (50 mL) and the solution was stirred vigorously at -78°C. Upon cooling, n-BuLi (5.75 mL, 9.2 mmol of a 1.6M solution in hexane) was slowly added. After 5 mins, a solution of bis(2-bromopyrid-6-yl)ketone (3.08 g, 9.0 mmol) in THF (100 mL) was transferred *via* cannula to the lithiated solution. The resulting solution was stirred at -78°C for 24 h and then allowed to warm to 0°C and was quenched with 10% aqueous K_2CO_3. The crude product was partitioned between $CHCl_3$ and water. The aqueous layer was washed twice with $CHCl_3$ (60 mL) and the organic layers were combined and dried with anhydrous $MgSO_4$. After filtration, the organic solvent was evaporated under reduced pressure. A dark brown oily crude product was obtained which crystallised on cooling. The crystals were washed with diethyl ether to give an off-white solid (45%). This was not always the case as sometimes the crude product had to be chromatographed on silica gel and eluted with DCM/MeOH (95:5) to give a white solid (55%). ^1H NMR ($CDCl_3$): δ 6.70 (s, 1H, O*H*), 7.15 (dd, 1H, *J* 6.5, 1.9 Hz), 7.30 (d, 2H, *J* 7.9 Hz), 7.45 (d, 2H, *J* 7.2 Hz), 7.65-7.70 (m, 4H), 8.45 (d, 1H, *J* 6.5 Hz); IR KBr/cm^{-1}: ν = 3411m, 1587s, 1562m, 1434m, 1413m, 1166s, 1140m, 989m, 807s, 761m, 712w; accurate EIMS (*m/z*): 419.9342 [M + H]$^+$.

Mono(2,2'-bipyrid-6-yl)bis(pyrid-2-yl)methanol, L^1

The starting materials mono(6-bromopyrid-2-yl) bis(pyrid-2-yl)methanol (1.209 g, 3.54 mmol), 2-tributylstannylpyridine (2.86 g, 7.08 mmol), and tetrakis(triphenylphosphane) palladium catalyst (Pd(PPh$_3$)$_4$) (0.82 g, 20% w/w) were dissolved in toluene (40 mL). The resulting mixture was stirred at 110°C under nitrogen for 24 h. The solution was cooled and toluene evaporated. The crude product (0.95 g, 75%) was chromatographed on silica gel and eluted initially with CH_3OH/DCM (1:99) to extract the excess 2-tributylstannylpyridine and finally flushed with CH_3OH/DCM (30:70). Evaporation of these latter fractions yielded a white solid (0.55 g, 55%). ^1H NMR ($CDCl_3$): δ 7.12 (dd, 1H, *J* 7.6, 3.0 Hz), 7.20 (dd, 2H, *J* 7.8, 4.8 Hz), 7.70 (m, 7H), 8.10 (dd, 1H, *J* 7.4, 3.2 Hz) 8.28 (dd, 1H, *J* 6.9, 5.4 Hz), 8.48 (d, 2H, *J* 7.8 Hz), 8.60 (d, 1H, *J* 7.0 Hz); IR KBr/cm^{-1}: ν = 3290m, 1581s, 1565s, 1458m, 1429s, 1394m, 1268w, 1059m, 993m, 774s, 738m. ESMS: *m/z* 341.1964 (100) [M + H]$^+$.

Bis(2,2'-bipyrid-6-yl)mono(pyrid-2-yl)methanol, L^2

Bis(6-bromopyrid-2-yl)mono(pyrid-2-yl) methanol (1.0 g, 2.4 mmol), 2-tributylstannylpyridine (3.84 g, 9.51 mmol) and Pd(PPh$_3$)$_4$ (0.55 g, 20% w/w) in toluene (40 mL) were reacted in the same manner as seen for ligand L^1. The crude product obtained (0.90 g, 75%) was chromoatographed on silica gel and again eluted with MeOH/DCM (1:99) to extract the excess 2-tributylstannylpyridine. The column was then flushed with MeOH/DCM (30:70) to yield a light brown solid (60%). ^1H NMR ($CDCl_3$): δ 7.12 (dd, 2H, *J* 7.6, 1.6 Hz), 7.20 (dd, 1H, *J*, 7.7, 5.7 Hz), 7.60 (t, 2H, *J* 7.7 Hz), 7.75 (m, 6H), 8.10 (dd, 2H, *J* 7.7, 2.8 Hz), 8.28 (dd, 2H, *J* 7.5, 6.0 Hz), 8.48 (d, 1H, *J* 7.5 Hz), 8.58 (d, 2H, *J* 6.5 Hz); ^{13}C NMR ($CDCl_3$): δ 85, 119, 120, 121, 122, 123, 130, 134, 136, 149, 150, 154, 159, 161 (N.B. two absent carbons); IR KBr/cm^{-1}: ν = 3310m, 1583s, 1569s, 1455m, 1431s, 1398m, 1271w, 1064m, 989m, 777s, 741m; ESMS: *m/z*; 418.2209 [M + H]$^+$.

General Procedure for the synthesis of metal complexes

The ligand (1 equivalent, 0.1 mmol) was dissolved in the minimum amount of acetonitrile or methanol (~3 mL). The solutions were warmed to *ca*. 60°C to ensure that the ligand fully dissolved. To this stirring solution, the metal perchlorate salt (1 equivalent) dissolved in either acetonitrile or water (~2 mL) was added dropwise. A precipitate was collected and dried in air. Recrystallisation of the compounds typically involved the diffusion of diethyl ether into acetonitrile or methanolic solutions which were filtered through Celite.

WARNING: Perchlorate salts of metal complexes are potentially explosive. Care should be taken while handling such complexes.

[Mn^{II}(L^1)(CH$_3$CN)(ClO$_4$)][ClO$_4$] (1): White precipitate (47% yield). Found: C, 43.58; H, 2.97; N, 11.09%. MnC$_{21}$H$_{16}$N$_4$O(ClO$_4$)$_2$·CH$_3$CN requires C, 43.48; H, 3.01; N, 11.02%; ESMS *m/z* (%): 609.06 (40) [Mn(L^1) + H$_2$O + ClO$_4$]$^+$; IR (KBr pellet, cm^{-1}): 3434(br), 3075(m), 1602(s), 1448(s) 1091(s), 777(s), 623(s); UV/Vis [λ$_{max}$, nm (ε$_M$, M^{-1}cm^{-}

^{1})] in CH$_3$CN: 242(22,460), 295(24,220), 316(8,070).

[Fe^{II}(L^1)][ClO$_4$]$_2$ (2) §: Dark orange precipitate (62% yield). HRMS (ES) *m/z* (%): 436.0881 (100) ([Fe(L^1) + CH$_3$CN - H]$^+$; FeC$_{23}$H$_{18}$N$_5$O requires 436.0861); IR (KBr pellet, cm^{-1}): 3372(br), 3113(m), 1599(s), 1450(s) 1095(s), 772(s), 623(s); UV/Vis [λ$_{max}$, nm (ε$_M$, M^{-1}cm^{-1})] in CH$_3$CN: 234(23,110), 287(22,550), 307(6,260), 482(19), 533(31).

[Co^{II}(L^1)(CH$_3$CN)][ClO$_4$]$_2$ (3): Bright orange precipitate (73% yield). Found: C, 43.92; H, 3.33; N, 11.55%. CoC$_{21}$H$_{16}$N$_4$O(ClO$_4$)$_2$·CH$_3$CN requires C, 43.21; H, 3.00; N, 10.96%; HRMS (ES) *m/z* (%): 399.0508 (100) ([Co(L^1)]$^+$; CoC$_{21}$H$_{16}$N$_4$O requires 399.0656); IR (KBr pellet, cm^{-1}): 3419(br), 3109(m), 1606(s), 1449(s), 1111(s), 770(s), 626(s); UV/Vis [λ$_{max}$, nm (ε$_M$, M^{-1}cm^{-1})] in CH$_3$CN: 233(19,510), 286(16,350), 459(150), 1051(28).

[Ni^{II}(L^1)(CH$_3$CN)(ClO$_4$)][ClO$_4$] (4): Light purple crystals (45% yield). Found: C, 43.32; H, 2.98; N, 11.03%. NiC$_{21}$H$_{16}$N$_4$O(ClO$_4$)$_2$·CH$_3$CN requires C, 43.23; H, 3.00; N, 10.96%; HRMS (ES) *m/z* (%): 438.0873 (100) ([Ni(L^1) + CH$_3$CN − H]$^+$; NiC$_{23}$H$_{18}$N$_5$O requires 438.0865); IR (KBr pellet, cm^{-1}): 3415(br), 3092(m) 1601(s), 1452(s), 1114(s), 767(s), 623(s); UV/Vis [λ$_{max}$, nm (ε$_M$, M^{-1}cm^{-1})] in CH$_3$CN: 265(21,850), 306(14,300), 714(67), 774(93).

[Cu^{II}(L^1)(H$_2$O)][ClO$_4$]$_2$·CH$_3$OH (5) §: Dark blue crystals (56% yield). HRMS (ES) *m/z* (%): 402.0535 (50) ([Cu(L^1) − H]$^+$; CuC$_{21}$H$_{15}$N$_4$O requires 402.0542); IR (KBr pellet, cm^{-1}): 3366(br), 3114(m), 1600(s), 1453(s), 1097(s), 776(s), 624(s); UV/Vis [λ$_{max}$, nm (ε$_M$, M^{-1}cm^{-1})] in CH$_3$CN: 251(23,700), 304.7(14,040), 317(9,200), 658(83), 920(37).

[Zn^{II}(L^1)(CH$_3$CN)(ClO$_4$)][ClO$_4$]·(6): White precipitate (68% yield). Found: C, 42.91; H, 3.05; N, 10.96%. ZnC$_{21}$H$_{16}$N$_4$O(ClO$_4$)$_2$·CH$_3$CN requires C, 42.78; H, 2.97; N, 10.85%; ^{1}H NMR (400 MHz; d$_6$-DMSO): 8.74 (d, 2H, *J* 7.0 Hz), 8.67 (d, 1H, *J* 7.0 Hz), 8.55 (m, 2H), 8.11 (dd, 2H, *J* 7.2, 6.9 Hz), 7.99 (dd, 1H, *J* 7.1, 5.0 Hz), 7.78 (d, 2H, *J* 7.0 Hz), 7.69 (t, 1H, *J* 5.4 Hz), 7.51 (d, 1H, *J* 7.1 Hz), 7.47 (t, 2H, *J* 6.9 Hz), 7.19 (dd, 1H, *J* 6.9, 5.4 Hz); HRMS (ES) *m/z* (%): 403.0520 (30) ([Zn(L^1) − H]$^+$; ZnC$_{21}$H$_{15}$N$_4$O requires 403.0537); IR (KBr pellet, cm^{-1}): 3319(br), 3093(m), 1595(s), 1454(s), 1098(s), 783(s), 622(s).

[Cd^{II}(L^1)(CH$_3$CN)(ClO$_4$)][ClO$_4$] (7): Colourless crystals (needles) (40% yield). Found: C, 40.08; H, 2.90; N, 10.30%. CdC$_{21}$H$_{16}$N$_4$O(ClO$_4$)$_2$·CH$_3$CN requires C, 39.88; H, 2.76; N, 10.11%; ^{1}H NMR (500 MHz; d$_6$-DMSO): 8.85 (d, 1H, *J* 7.0 Hz), 8.62 (d, 2H, *J* 6.4 Hz), 8.57 (t, 1H, *J* 7.4 Hz), 8.53 (d, 1H, *J* 6.6 Hz), 8.37 (bs, 2H), 8.34-8.25 (m, 4H), 8.11 (d, 2H, *J* 6.4 Hz), 7.92 (t, 1H, *J* 7.0 Hz), 7.61 (t, 2H, *J* 6.8 Hz); ^{13}C NMR: (125 MHz; d$_6$-DMSO): 159.7, 159.0, 150.1, 149.5, 148.7, 148.6, 141.8, 141.0, 140.3, 126.7, 124.2, 123.0, 121.8, 121.7, 75.1; HRMS (ES) *m/z* (%): 490.0552 (30) ([Cd(L^1) + CH$_3$CN + H]$^+$; CdC$_{23}$H$_{18}$N$_5$O requires 490.0541); IR (KBr pellet, cm^{-1}): 3320(br), 3093(m), 1595(s), 1454(s), 1098(s),

800(s), 622(s).

[Mn^{II}(L^2)(CH$_3$CN)][ClO$_4$]$_2$. 2CH$_3$CN (8): Pale yellow crystals (88% yield). Found: C, 48.51; H, 3.71; N, 14.28%. MnC$_{26}$H$_{19}$N$_5$O(ClO$_4$)$_2$·3CH$_3$CN requires C, 48.38; H, 3.55; N, 14.10%; ESMS *m/z* (%): 472.1 (100) [Mn(L2) + H]$^+$; IR (KBr pellet, cm^{-1}): 3367(br), 3087(m), 1603(s), 1449(s), 1117(s), 779(s), 623(s); UV/Vis [λ$_{max}$, nm (ε$_M$, M^{-1}cm^{-1})] in CH$_3$CN: 234(23,500), 292(16,600), 314(7,100).

[Fe^{II}(L^2)(CH$_3$CN)][ClO$_4$]$_2$·Et$_2$O (9): Purple crystals (55% yield). Found: C, 49.58; H, 4.29; N, 11.90%. FeC$_{26}$H$_{19}$N$_5$O(ClO$_4$)$_2$·2CH$_3$CN·(CH$_3$CH$_2$)$_2$O requires C, 49.29; H, 4.26; N, 11.84%; ESMS *m/z* (%): 571.74 (100) [Fe(L^2) + ClO$_4$]$^+$; IR (KBr pellet, cm^{-1}): 3425(br), 3109(m), 1602(s), 1450(s), 1109(s), 777(s), 624(s); UV/Vis [λ$_{max}$, nm (ε$_M$, M^{-1}cm^{-1})] in CH$_3$CN: 239(20,250), 295(18,450), 316(4,400), 419(112), 504(78), 577(133).

[Co^{II}(L^2)(CH$_3$CN)][ClO$_4$]$_2$·0.5H$_2$O (10): Dark orange crystals (33% yield). Found: C, 45.81; H, 2.36; N, 11.50%. CoC$_{26}$H$_{19}$N$_5$O(ClO$_4$)$_2$·CH$_3$CN·H$_2$O requires C, 45.79; H, 3.29; N, 11.44%; HRMS (ES) *m/z* (%): 575.0406 (50) ([Co(L^2) + ClO$_4$]$^+$; CoC$_{26}$H$_{19}$ClN$_5$O$_5$ requires 575.0407); IR (KBr pellet, cm^{-1}): 3398(br), 3115(m), 1599(s), 1451(s), 1105(s), 779(s), 623(s); UV/Vis [λ$_{max}$, nm (ε$_M$, M^{-1}cm^{-1})] in CH$_3$CN: 231(23,800), 284(19,850), 302(4,150), 463(103), 1030(21).

[Ni^{II}(L^2)(Br)][ClO$_4$] (11) §: Dark purple crystals (71% yield). ESMS *m/z* (%): 575.2 (100) [Ni(L^2) + ClO$_4$]$^+$; IR (KBr pellet, cm^{-1}): 3388(br), 3110(m), 1602(s), 1450(s), 1088(s), 782(s), 625(s); UV/Vis [λ$_{max}$, nm (ε$_M$, M^{-1}cm^{-1})] in CH$_3$CN: 248(22,000), 298(21,500), 312(9,150), 512(19), 820(15), 956(11).

[Cu^{II}(L^2)(CH$_3$CN)][ClO$_4$]$_2$ (12): Light blue precipitate (62% yield). Found: C, 46.73; H, 3.04; N, 11.75%. CuC$_{26}$H$_{19}$N$_5$O(ClO$_4$)$_2$·CH$_3$CN requires C, 46.65; H, 3.08; N, 11.66%; ESMS *m/z* (%): 580.1 (100) [Cu(L^2) + ClO$_4$]$^+$; IR (KBr pellet, cm^{-1}): 3434(br), 3095(m), 1595(s), 1453(s), 1095(s), 780(s), 624(s); UV/Vis [λ$_{max}$, nm (ε$_M$, M^{-1}cm^{-1})] in CH$_3$CN: 245(20,750), 301(29,300), 316(10,300), 639(54).

[Zn^{II}(L^2)][ClO$_4$]$_2$·Et$_2$O (13): White precipitate (80% yield). Found: C, 48.48; H, 4.21; N, 10.68%. ZnC$_{26}$H$_{19}$N$_5$O(ClO$_4$)$_2$·CH$_3$CN·(CH$_3$CH$_2$)$_2$O requires C, 48.23; H, 4.05; N, 10.55%; ^{1}H NMR (400 MHz; d$_6$-DMSO): 8.72 (d, 1H, *J* 7.0 Hz), 8.65 (d, 2H, *J* 7.0 Hz), 8.56 (m, 4H) 8.08 (dd, 1H, *J* 7.2, 6.9 Hz), 7.99 (dd, 2H, *J* 7.1, 5.0 Hz), 7.79 (d, 1H, *J* 7.0 Hz), 7.70 (t, 2H, *J* 5.4 Hz), 7.53 (d, 2H, *J* 7.1 Hz), 7.45 (t, 1H, *J* 6.9 Hz), 7.19 (dd, 2H, *J* 6.9, 5.4 Hz); ^{13}C NMR: (125 MHz; CD$_3$CN): 157.2, 157.1, 149.0, 148.6, 148.3, 142.4, 141.6, 140.7, 127.2, 124.4, 122.7, 122.2, 121.3, 120.8, 74.8; ESMS *m/z* (%): 581 (100) [Zn(L^2) + ClO$_4$]$^+$; IR (KBr pellet, cm^{-1}): 3427(br), 3115(m), 1598(s), 1451(s) 1108(s), 779(s), 624(s).

[Cd^{II}(L^2)(CH$_3$CN)][ClO$_4$]$_2$, 2CH$_3$CN (14): Colourless crystals (needles) (77% yield). Found: C, 45.20; H, 3.42; N, 13.18%. CdC$_{26}$H$_{19}$N$_5$O(ClO$_4$)$_2$·3CH$_3$CN requires C, 45.11; H, 3.31; N, 13.15%; ^{1}H NMR (250 MHz; CD$_3$CN): 9.29 (d, 2H, 6.30 Hz),
5 9.03 (d, 1H, J 6.10 Hz), 8.40-8.53 (m, 6H), 8.27-8.35 (m, 5H), 8.18 (t, 1H, J 7.4 Hz), 7.93 (t, 2H, J 7.6 Hz), 7.67 (t, 1H, J 6.8 Hz), 6.49 (s, 1H); ^{13}C NMR: (125 MHz; CD$_3$CN): 158.4, 158.2, 149.7, 149.2, 149.1, 148.6, 141.8, 141.2, 140.7, 127.0, 124.4, 123.2, 123.1, 122.1, 121.6, 75.2; HRMS (ES) m/z (%):
10 530.0566 (100) ([Cd(L^2) + H]$^+$; CdC$_{26}$H$_{18}$N$_5$O requires 530.0545); IR (KBr pellet, cm^{-1}): 3398(br), 3114(m), 1595(s), 1448(s), 1097(s), 779(s), 623(s).

§Despite numerous crystallisations and attempts to obtain suitable elemental analysis, we were unable to obtain data consistent with our
15 formulation. Accurate mass spectrometry was obtained for **2** and **5**, and the IR spectrum of crystals used to obtain the structures of **5** and **11** were consistent with the IR of the bulk sample.

Results and Discussion

Ligand Synthesis

20 The synthesis of L^1 and L^2 have recently been reported by Alberto,[12,13] by the addition of the lithiated 6-bromo-2,2'-bipyridine to the appropriate ketone (2,2-dipyridylketone or 2-pyridine-6-(2,2'-bipyridyl)ketone). Alternatively, we have found these ligands may be synthesised via the bromo
25 substituted tripodal ligands. The preparation of ligands L^1 and L^2 have been summarised in Scheme 1 and the bromo derivatives were readily prepared in reasonable yields.[15] As such, these precursors may be utilised in the synthesis of a range of tripodal ligands via Stille coupling or palladium
30 catalysed carbonylation reactions. To couple the bromopyridine with another pyridine group, the respective bromo derivative was suspended in toluene and treated with an excess of 2-tributylstannylpyridine in the presence of the palladium catalyst, Pd(PPh$_3$)$_4$, for 24 hours at 110°C to
35 generate the respective bipy derivative. The crude products of L^1 and L^2 were flash chromatographed on silica gel. Initially, the column was flushed with CH$_2$Cl$_2$:MeOH (99:1) to extract the excess 2-tributylstannylpyridine and finally with MeOH (30%) to obtain the desired product, mono(2,2'-bipyrid-6-
40 yl)bis(2-pyridyl)methanol, L^1, as a white solid (55%) and bis(2,2'-bipyrid-6-yl)mono(2-pyridyl)methanol, L^2, as a light brown solid (60%).[16]

Synthesis of Complexes

The ligand was dissolved in the minimum amount (~3 mL) of
45 warm acetonitrile. In each case, the dropwise addition of the relevant metal perchlorate salt dissolved in either water or acetonitrile instantly yielded a precipitate. These compounds were recrystallised via the diffusion of diethyl ether into acetonitrile or methanolic solutions resulting in crystals
50 suitable for single-crystal X-ray diffraction. The yields from these reactions were moderate to high (41-87%).

Spectroscopic Properties of Complexes

Vibrational Spectroscopy

The transition metal complexes of ligands L^1 and L^2 reveal a
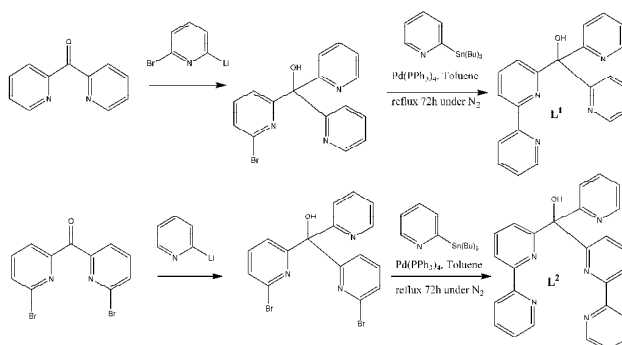
55 variety of diagnostic vibrations indicative of pyridine co-ordination to a metal centre. Upon complexation a shift of the strong 1580 cm^{-1} band to higher frequency (*ca.* 1600 cm^{-1}) was observed. Such a shift reflects the more rigid nature of complex in comparison to the free ligand. The unsplit infrared
60 **Scheme 1** Synthetic route to ligands L^1 and L^2

active bands at 1087-1116 cm^{-1} and ~623 cm^{-1} indicate the perchlorate counterions are of T$_d$ symmetry and therefore non-coordinating, which is in accordance with the X-ray
65 diffraction data.

^{1}H and ^{13}C NMR of Zn and Cd Complexes

The ^{1}H NMR spectra of the zinc complexes of L^1 and L^2 yield sharp well-defined spectra that are both highly comparable to
70 their parent ligands. However, the protons in the zinc complexes are more deshielded and the corresponding signals appear at more downfield positions, particularly for protons ortho to the co-ordinating nitrogen atoms. As might be expected, the two pyridyl units in L^1 are equivalent, as is the
75 case for the two bipyridyl units of L^2. For the cadmium complex of L^1, it is apparent that the ordering of the signals is different on comparison to both the parent ligand and analogous zinc complex.
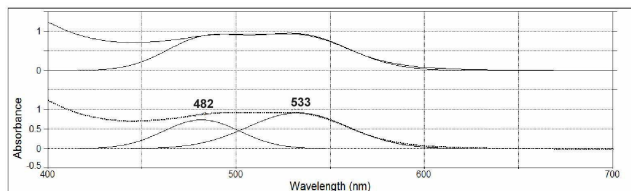
Electronic Absorption Spectra

80 The electronic absorption spectra for all complexes of L^1 and L^2 possess two strong peaks between 231 nm and 306 nm characteristic of intra-ligand bipyridine π-π* transitions.
The Fe^{II} complex of L^1 contains a band in the visible region at
85 533 nm which has a shoulder at higher energy. Deconvolution of the spectra with PeakFit v4.12 reveals the shoulder reaches its absorbance maximum at 482 nm (Fig. 2). Ligand L^1 has been shown by X-ray diffraction studies to form both trigonal bipyramidal (Cu^{II}) and octahedral (Ni^{II}, Cd^{II}) co-ordination
90 geometries in the solid state. For Fe(II) complexes, both high-spin trigonal bipyramidal and high-spin six co-ordinate C$_{2v}$ complexes give similar spectra. Typically both high spin trigonal bipyramidal (HS TBP) and six coordinate C$_{2v}$ complexes give two bands at very low energy (1000-2000
95 nm). For example, in the complex, *cis*-Fe^{II}py$_4$Cl$_2$, these bands are observed at the much lower energies of 951 and 1147 nm.[17,18] An alternative scenario is that of a low-spin pseudo-octahedral geometry. In such cases, two transitions (^{1}A$_{1g}$→^{1}T$_{1g}$ and ^{1}A$_{1g}$→^{1}T$_{2g}$) are typically seen. In some cases,
100 a third transition attributable to the spin-forbidden triplet state

Table 1: Electronic spectral assignments[a] for complexes **1-5** and **8-12**

Compound	π-π^* transitions / λ (nm)	MLCT / λ (nm)	d-d transitions / λ (nm)	Δ (cm^{-1})[b]	B' (cm^{-1})[b]
[Mn^{II}(L^1)(CH$_3$CN)(ClO$_4$)] [ClO$_4$] (**1**)	242(22,460), 295(24,220)	316(8,070)	-	-	-
[Fe^{II}(L^1)][ClO$_4$]$_2$ (**2**)	234(23,110), 287(22,550)	307(6,260)	482(19), 533(31)	-	-
[Co^{II}(L^1)(CH$_3$CN)(ClO$_4$)] [ClO$_4$] (**3**)	233(19,510), 286(16,350)	-	459(150), 1051(28)	10,800	900
[Ni^{II}(L^1)(CH$_3$CN)(ClO$_4$)] [ClO$_4$] (**4**)	265(21,850), 306(14,300)	-	509(78), 779(67), 884(93)	12,830	778
[Cu^{II}(L^1)(H$_2$O)] [ClO$_4$]$_2$(CH$_3$OH) (**5**)	251(23,700), 305(14,040)	317(9,200)	658(83), 920(37)	-	-
[Mn^{II}(L^2)(CH$_3$CN)] [ClO$_4$]$_2$ (**8**)	234(23,500), 292(16,600)	314(7,100)	-	-	-
[Fe^{II}(L^2)(CH$_3$CN)] [ClO$_4$]$_2$ (**9**)	239(20,250), 295(18,450)	316(4,400)	419(112), 504(78), 577(133)	-	-
[Co^{II}(L^2)(CH$_3$CN)] [ClO$_4$]$_2$ (**10**)	231(23,800), 284(19,850)	302(4,150)	463(103), 1030(21)	11,000	880
[Ni^{II}(L^2)(Br)] [ClO$_4$] (**11**)	248(22,000), 298(21,500)	312(9,150)	512(19), 820(15), 956(11)	12,195	950
[Cu^{II}(L^2)(CH$_3$CN)] [ClO$_4$]$_2$ (**12**)	245(20,750), 301(29,300)	316(10,300)	639(54)	-	-

[a]performed in CH$_3$CN solution at room temperature; Numbers in parentheses indicate molar absorption coefficients ε (M^{-1}cm^{-1}). [b]values calculated by assuming an octahedral geometry

Fig. 2 Deconvolution of the Electronic Spectrum of the Fe^{II} complex of L^1

[5] ^{3}T$_1$ is also reported. The compound, c-Fe^{II}Cl$_2$(ArNC)$_4$ presents absorption bands at 437 and 575 nm corresponding to the two spin-allowed transitions.[19] The analogous Fe^{II} complex of L^2 has three bands within the visible region at 419, 504 and 577 nm (Fig. 3). Single crystal X-ray diffraction [10] studies of the compound reveal a distorted octahedral co-ordination geometry with short Fe-N distances typical of low spin complexes, however, the electronic spectra is uncharacteristic of either high spin or low spin d^6 octahedral complexes.

[15] The complex [Co^{II}(L^1)(CH$_3$CN)(ClO$_4$)][ClO$_4$] contains two bands in the visible region of its electronic spectrum at 459 and 1051 nm, characteristic of a high-spin octahedral Co^{II} complex. High-spin complexes of d^7 ions may show three spin-allowed transitions; the lowest energy transition is [20] attributed to ^{4}T$_{1g} \rightarrow$ ^{4}T$_{2g}$ which usually appears at *ca.* 1000 - 1250 nm. The second transition, assigned to ^{4}T$_{1g} \rightarrow$ ^{4}T$_{1g}$(P) , typically appears at *ca.* 500 nm. As in this instance, the other spin-allowed transition, ^{4}T$_{1g} \rightarrow$ ^{4}A$_{2g}$, is not always observed. The ratio ν_1/ν_2 is 0.437 which suggests Δ/B = 11.94. Thus, B =

[25] 900 cm^{-1} and Δ = 10,800 cm^{-1}. The high-spin Co^{II} octahedral complex, [Co(py)$_6$]$^{2+}$, has absorptions at 490 and 1020 nm.[20]

The Co^{II} complex of L^2 reveals two bands in the NIR/visible region at 1030 and 463 nm. In the solid state, this complex has slightly more trigonal prismatic content than [30] octahedral (see Table 7 for results of CShM calculations), however the difference is only minor and the electronic spectrum is very similar to that seen for the analogous Co^{II} complex of L^1. Therefore, the observed transitions have been assigned in an identical manner. The ratio ν_1/ν_2 is 0.450 and, [35] Δ/B = 12.51. Thus, B = 880 cm^{-1} and Δ = 11,000 cm^{-1}. If the complex maintained predominantly trigonal prismatic character in solution one would expect further splitting of the observed absorption bands in the visible region. Previous examples observed three absorption bands corresponding to [40] the transitions: ^{4}E' $\rightarrow$ ^{4}E" + ^{4}A$_2$' + ^{4}A$_1$", ^{4}A$_2$" (unresolved), ^{4}E' $\rightarrow$ ^{4}E"(P), and ^{4}E' $\rightarrow$ ^{4}A$_2$'(P) at approximately 1185, 525 and 450 nm respectively.[6]
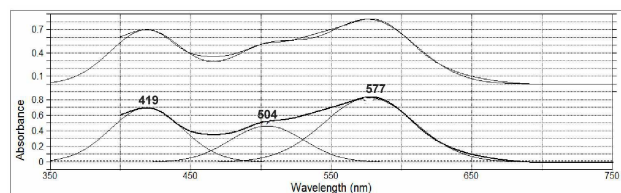
Fig. 3 Deconvolution of the Electronic Spectrum of the Fe^{II} complex of L^2

The complex [Ni^{II}(L^1)(ClO$_4$)][ClO$_4$] reveals two regions of

absorption in the visible region of its electronic spectrum (Fig. 4). One absorbance maxima occurs at 509 nm, and analysis of the second region reveals two overlapping peaks at 884 and 779 nm. The CShM results derived from the crystallographic data indicate an 'octahedral' co-ordination geometry, which due to the differing donor atoms, is best described as having pseudo-C_{2v} symmetry.
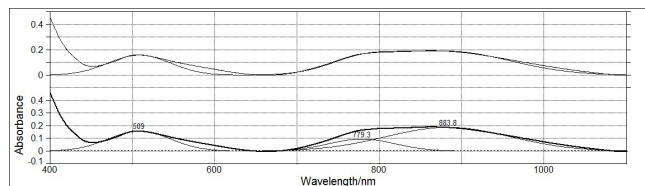

Fig. 4 Deconvolution of the Electronic Spectrum of the Ni^{II} complex of L^1

Three spin-allowed absorption bands are expected in octahedral complexes, corresponding to transitions from $^3A_{2g}$ to $^3T_{2g}$, $^3T_{1g}$ and $^3T_{1g}(P)$ from lowest to highest energy respectively. These three bands are typically observed in the regions 770 – 1430 nm, 500-900 nm and 370-520 nm. For example, the related complex $[Ni(bipy)_3]^{2+}$ reveals three transitions at 790, 520 and 385 nm.[20] The visible region of $[Ni(bipy)_3]^{2+}$ also reveals one further transition at 870 nm which corresponds to the spin-forbidden transition to ^1E_g. Treating the molecule as possessing octahedral symmetry we may assign the peaks at 884, 779 and 509 nm as $^1A_{2g} \rightarrow {}^3E_g$, $^3A_{2g} \rightarrow {}^3T_{2g}$, and $^3A_{2g}(F) \rightarrow {}^3T_{1g}(F)$ with the $^3A_{2g} \rightarrow {}^3T_{1g}(P)$ transition being obscured by charge transfer bands. However, allowing for the lower pseudo-C_{2v} symmetry of the complex, the spectrum may be reassigned. The band at 779 nm has been ascribed to the second spin-allowed transition $^3B_{1g} \rightarrow {}^3A_{2g}+{}^3B_{2g}$ and the shoulder at 884 nm to the spin-forbidden transition $^3B_{1g} \rightarrow {}^1B_{1g}(D)+{}^1A_{1g}(D)$ The third band in the visible region at 509 nm has been attributed to the transition $^3B_{1g} \rightarrow {}^3B_{2g}$. There are several additional spin-allowed transitions which occur at higher energy which are most likely obscured by charge transfer bands or ligand-based processes. The lowest energy transition $^3B_{1g} \rightarrow {}^3A_{1g}$ most likely occurs in the near-infrared region, outside the operating range of the spectrophotometer.

The Ni^{II} complex of L^2 was initially prepared by the addition of $[HL^2]Br$ to $[Ni(H_2O)_6](ClO_4)_2$ yielding $[NiL^2(Br)][ClO_4]$. However, the *in situ* preparation of the bromide free complex, by addition of L^2 to $[Ni(H_2O)_6](ClO_4)_2$ in acetonitrile yielded a solution with an identical electronic spectrum. In addition the spectrum was very similar to that of the Ni^{II} complex of L^1. There is one absorbance maximum which occurs at 512 nm, and deconvolution of the second region reveals two overlapping peaks at 920 and 658 nm. Again, as this complex exhibits a predominantly 'octahedral' co-ordination environment with C_{2v} symmetry, the absorption bands may be tentatively assigned in an identical manner to the preceding complex.

The complex $[Cu^{II}(L^1)(CH_3CN)(ClO_4)][ClO_4]$ contains two broad absorption bands in the visible region at 658 and 920 nm (Fig. 5). Single crystal X-ray diffraction data indicates the

five-coordinate geometry surrounding the metal centre lies almost exactly halfway between trigonal bipyramidal and square pyramidal. The absorption pattern expected for a trigonal bipyramidal copper complex involves peaks extending from *ca.* 685 - 950 nm with a greater absorption intensity proceeding from higher to lower energy. However, square pyramidal environment would lead to a similar band envelope in the range *ca.* 660 – 880 nm, however in this case the absorption intensity is expected to increase to higher energy as seen in $K[Cu(NH_3)_5][PF_6]_3$.[21] Compound **5** does indeed show this intensity pattern perhaps suggesting square pyramidal coordination geometry. Alternatively, in solution, $[Cu^{II}(L^1)(CH_3CN)(ClO_4)][ClO_4]$ may form an octahedral co-ordination environment with C_{2v} symmetry in solution. In this case the one electron energy sequence of the Cu^{II} ion is approximately the same as that predicted for the square-based pyramidal geometry, *i.e.* $(x^2-y^2) > (z^2) > (xy) > (xz) \approx (yz)$. Therefore, the broad absorption band at higher energy may be tentatively assigned to transitions from components of t_{2g}, *i.e.* $(xy, xz \approx yz) \rightarrow (x^2-y^2)$, and the lower energy band as $(z^2) \rightarrow (x^2-y^2)$ transitions. A pertinent example is that of $Cu(bipy)_2(ONO)^+$ which reveals two bands at 1052 and 671 nm, corresponding to the transitions $(z^2 \rightarrow x^2-y^2)$ and $(xy, xz \approx yz \rightarrow x^2-y^2)$.[22]

The analogous Cu^{II} complex of L^2 presents a very typical octahedral Cu^{II} electronic spectrum *i.e.* a single poorly resolved broad peak in the visible region (639 nm). Here, the unstable ^2E_g ground state resulting from the asymmetrical filling of the degenerate anti-bonding E_g subset of orbitals causes a tetragonal distortion. The ^2E_g term splits into $^2B_{1g}$ and $^2A_{1g}$, and the $^2T_{2g}$ term splits into $^2B_{2g}$ and ^2E_g. Therefore, two overlapping bands corresponding to the transitions $^2B_{1g} \rightarrow {}^2B_{2g}$ and $^2B_{1g} \rightarrow {}^2E_g$ are seen in the visible region, while the $^2B_{1g} \rightarrow {}^2A_{1g}$ is of lower energy and is typically observed in the near infra red. In this instance, identification of these transitions *via* de-convolution could not be performed with confidence owing to the broad symmetrical nature of the absorption band.
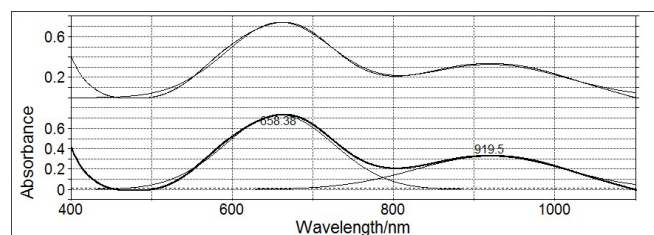

Fig. 5 Deconvolution of the Electronic Spectrum of the Cu^{II} complex of Ligand L^1

Table 2 Crystal structure data for complexes **4, 5, 7, 8, 9, 10** and **14**

Compound	**4**	**5**	**7**	**8**	**9**	**10**	**14**
Chemical Formula	$[Ni^{II}(L^1)(ClO_4)(CH_3CN)]$ $[ClO_4]$	$[Cu^{II}(L^1)(H_2O)]$ $[ClO_4]_2(CH_3OH)_2$	$[Cd^{II}(L^1)(ClO_4)(CH_3CN)]$ $[ClO_4]$	$[Mn^{II}(L^2)(CH_3CN)]$ $[ClO_4]_2(CH_3CN)$	$[Fe^{II}(L^2)(CH_3CN)]$ $[ClO_4]$ (CH_3CN)	$[Co^{II}(L^2)(CH_3CN)]$ $[ClO_4]_2$ $0.5(H_2O)$	$[Cd^{II}(L^2)(CH_3CN)]$ $[ClO_4]_2$ (CH_3CN)
Mr, gmol^{-1}	639.04	684.92	692.73	753.41	754.32	1450.71	810.87
Crystal System	Orthorhombic	Triclinic	Orthorhombic	Monoclinic	Triclinic	Monoclinic	Monoclinic
Space group	Pbca	P-1	Pbca	P2$_1$/n	P-1	P2$_1$/$_C$	P2$_1$/n
a, Å	12.871(3)	8.5840(17)	17.018(3)	12.7935(3)	10.1576(2)	14.0840(2)	12.8927(2)
b, Å	16.309(3)	11.785(2)	12.700(3)	12.3606(3)	11.9556(3)	21.3004(3)	12.4047(3)
c, Å	23.680(5)	14.702(3)	23.847(5)	20.9431(6)	15.5564(5)	19.6325(3)	20.9303(5)
α, deg	90	96.70(3)	90	90	95.1700(10)	90	90
β, deg	90	96.70(3)	90	101.7290(10)	100.1480(10)	94.2450(10)	102.3110(10)
γ, deg	90	109.93(3)	90	90	93.0010(10)	90	90
Z	8	2	8	4	2	4	4
Dc, Mg/m^3	1.708	1.662	1.786	1.543	1.356	1.641	1.647
μ(Mo Kα), mm^{-1}	1.061	1.064	1.118	0.637	0.610	0.835	0.896
Reflections Collected	23795	24985	24358	24477	29866	78539	25129
Unique Reflections	5680	6212	5876	7353	8315	13449	7447
R_{int}	0.0974	0.1141	0.0756	0.0933	0.0998	0.1788	0.0785
R_1 [$I>2\sigma(I)$]	0.0535	0.0503	0.0412	0.0578	0.0759	0.0640	0.0497
wR_2 (all data)	0.1319	0.1329	0.1048	0.1585	0.2257	0.1689	0.1254

Crystallographic Studies

X-ray data were collected on a Nonius Kappa CCD diffractometer at 150 K using graphite monochromated Mo-Kα radiation ($\lambda = 0.71073$ Å). The structures were solved using direct methods, with absorption corrections being applied as part of the data reduction scaling procedure.[23] Full least-square refinement was carried out on F^2. After refinement of the heavy atoms, difference Fourier maps revealed the maxima of residual electron density close to the positions expected for the hydrogen atoms; they were introduced as fixed contributors in the structure factor calculations with fixed coordinates and isotropic temperature factors, but were not refined. Hydrogen atoms bonded to the apical oxygen of the ligands, or the oxygen of methanol, were positioned in idealised positions (tetrahedral X–O–H) placing the hydrogens close to maxima in electron density; the O–H distances were allowed to refine but were restrained to 0.84 Å. Hydrogen atoms bonded to oxygen of water were located in the Fourier difference map and were refined with O–H

distance restrained to 0.84 Å. Hydrogen bonds were located and were refined where appropriate. The structure of **9** contained a highly disordered, non-co-ordinated, diethyl ether molecule. Attempts were made to model the disorder, but such attempts were unsuccessful and gave unrealistic and unacceptable bond distances and angles. Based upon this evidence, it was felt that an atomic model was unsuitable and the disordered region was modelled using SQUEEZE.[24] In several instances, perchlorate anions were disordered; the ions were modelled as two-site disorder. In these cases, 1,3-distance and thermal similarity restraints were applied and the refinement proceeded without further complications. A final difference map revealed no significant maxima of residual electron density. The scattering factor coefficients and the anomalous dispersion coefficients were taken from standard sources.[25] Structure solution and refinement were performed using the SHELX software suite.[26] Crystal data and experimental details are provided in Table 2. Molecular structures in the figures were drawn with ORTEP 3.0 for Windows (version 1.08).[27]

Crystal Structure of [Ni^{II}(L^1)(ClO$_4$)(CH$_3$CN)][ClO$_4$] (4)

The Ni^{II} complex of L^1 crystallises in the orthorhombic space group Pcab with one molecule in the asymmetric unit (Fig. 6). The Ni^{II} ion lies at the centre of a significantly distorted octahedral environment (*S(Oh)* = 1.45 *vs* *S*(TP) = 10.67) and is co-ordinated by two types of donor atom: five nitrogens and one oxygen. All four pyridyl N-donors are involved in co-ordination to the metal, the fifth nitrogen donor (N(5)) is located on an acetonitrile molecule and the oxygen donor (O(2)) originates from a perchlorate counterion. This donor set is identical to the analogous Cd^{II} complex, **7**. One commonly encountered distortion from Oh symmetry is due to the acute bite angle of the bipyridine ligand (N(3)-Ni(1)-N(4) (78.69(11)°)) varying significantly from 90°. Further distortions involve the bond angles between the three mutually *trans* sets of donor atoms, N(2)-Ni(1)-N(4) (163.52 (11)°), N(1)-Ni(1)-O(2) (169.56(10)°) and N(3)-Ni(1)-N(5) (173.03(12)°) which all deviate from the theoretical 180°. The mean average of the co-ordinative bond angles between the three pyridines which are directly attached to the methine bridge is 86.59(11)°, which indicates some degree of steric strain caused by the compact linking group (C(1)). All but one of the pyridyl N-Ni^{II} bond lengths closely resemble those of the similar octahedral compound (2,6-bis(1,1-bis(pyridin-2-yl)ethyl)pyridine)-(acetonitrile)-nickel^{II} bis(hexafluoro-phosphate) which exhibits pyridyl N-Ni^{II} bond lengths ranging from 2.049(5) Å to 2.111(5) Å.[28] The Ni(1)-N(3)
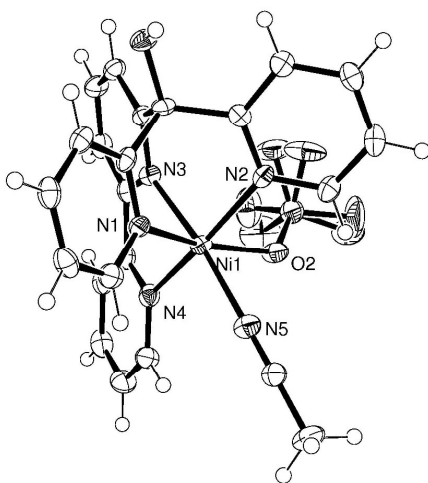

Fig .6 Perspective view of the asymmetric unit of **4** showing the atom numbering. Displacement ellipsoids are shown at the 50% probability level. H atoms are represented by circles of arbitrary size.

bond length in **4** is significantly shorter (2.009(3) Å) than the others. This is presumably caused by the N(4)/C(17)-C(21) pyridine ring wrapping around to co-ordinate to the Ni^{II} ion, forcing N(3) to adopt a closer position to the metal. The oxygen donor (O(2)) lies at a notably longer distance from the nickel centre (2.226(2) Å) in comparison to the nitrogen donor atoms, which again leads to deviation away from a regular octahedron in which all bond lengths are identical, however this longer Ni-O bond is typical for the weaker ClO$_4^-$ donor.

Table 3 Significant Bond lengths (Å) and Angles (°) for [Ni^{II}(L^1)(ClO$_4$)(CH$_3$CN)][ClO$_4$] (4)

Ni(1)-N(1)	2.068(3)	Ni(1)-N(4)	2.076(3)
Ni(1)-N(2)	2.057(3)	Ni(1)-N(5)	2.046(3)
Ni(1)-N(3)	2.009(3)	Ni(1)-O(2)	2.226(2)
N(3)-Ni(1)-N(5)	173.03(12)	N(2)-Ni(1)-N(4)	163.52(11)
N(3)-Ni(1)-N(2)	91.77(11)	N(1)-Ni(1)-N(4)	108.15(11)
N(5)-Ni(1)-N(2)	95.17(11)	N(3)-Ni(1)-O(2)	97.39(10)
N(3)-Ni(1)-N(1)	84.16(11)	N(5)-Ni(1)-O(2)	83.86(10)
N(5)-Ni(1)-N(1)	95.85(11)	N(2)-Ni(1)-O(2)	85.75(10)
N(1)-Ni(1)-N(2)	83.88(11)	N(1)-Ni(1)-O(2)	169.56(10)
N(3)-Ni(1)-N(4)	78.69(11)	N(4)-Ni(1)-O(2)	82.25(10)
N(5)-Ni(1)-N(4)	94.73(12)		

Crystal Structure of [Cu^{II}(L^1)(H$_2$O)][ClO$_4$]$_2$·(CH$_3$OH)$_2$ (5)

The Cu^{II} complex of L^1 crystallises in the triclinic space group P-1 with one complex within the asymmetric unit (Fig. 7). The Cu^{II} cation lies at the centre of a distorted trigonal bipyramidal co-ordination geometry consisting of four pyridyl N-donors (N(1)–N(4)) and an oxygen donor (O2) located on a solvent water molecule. The continuous shape measures (*S*(TBPY) = 3.35 and *S*(SPY) = 3.38) indicate this structure is intermediate to trigonal bipyramidal (TBPY) and square pyramidal geometries (SPY).

When consider TBP, the trigonal plane will be defined by N(1), N(2) and N(4). The most significant distortions involve the angles in this plane: the most acute angle is N(1)-Cu(1)-N(2) (86.48(10)°), while the most obtuse is N(2)-Cu(1)-N(4) (146.84(10)°). In order to generate a regular trigonal bipyramid, *i.e.* in which these angles correspond to the theoretical 120°, it would be necessary for the pyridine rings N(1)/C2-C6 and N(2)/C7-C(11) to lie closer to ring N(4)/C(17)-C(21). Such movement is prevented by the rigid framework of the ligand; specifically, the bonds C2-C(1) and C7-C(1), *i.e.* the immediate bonds connecting both pyridines to the methine bridge, would be required to lengthen in order to satisfy this criteria. Furthermore, the bond angles surrounding C(1) which indicate sp^3 hybridisation would be required to distort significantly away from the idealised angles which are maintained in the present conformation. The angle between the two axial donors N(3) and O2 (175.91(10)°) is only modestly less obtuse than the theoretical 180°. An example of a similar five co-ordinate structure which interestingly has been described as containing a 'square-based pyramidal distorted trigonal bipyramidal (SBPDTB) CuN$_4$O chromophore' is the compound aqua-bis(1,10-phenanthroline)-copper(II) diperchlorate.[29] Here, the pyridyl N-Cu^{II} bond lengths range from 1.980(4) Å to 2.032(4) Å which compares well with those found in compound **5**. Interestingly, the aqua O-Cu^{II} bond lengths are 2.245(4) Å which are significantly longer than that found in **5** (1.946(2) Å).
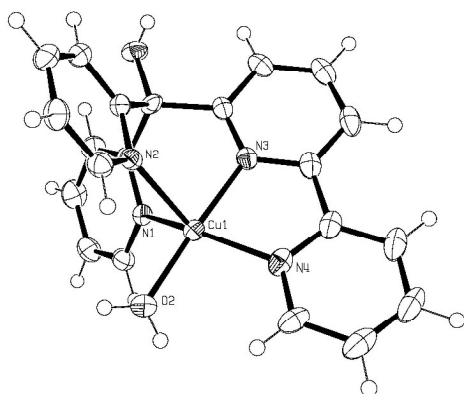
Fig. 7 Perspective view of the asymmetric unit of **5** showing the atom numbering. Displacement ellipsoids are shown at the 50% probability level. H atoms are represented by circles of arbitrary size.

Crystal Structure of [Cd^{II}(L^1)(ClO$_4$)(CH$_3$CN)][ClO$_4$] (7)

5 The Cd^{II} complex of L^1 crystallises in the orthorhombic space group Pcab with one complex within the asymmetric unit. The Cd^{II} ion lies at the centre of a significantly distorted octahedral geometry (S(Oh) = 3.95, S(TP) = 7.15) and is co-ordinated by four pyridyl N-donors (N(1)-N(4)), one solvent

10 **Table 4** Significant Bond lengths (Å) and Angles (°) for [Cu^{II}(L^1)(H$_2$O)][ClO$_4$]$_2$·(CH$_3$OH) (**5**)

Cu(1)-N(1)	2.061(3)	Cu(1)-N(4)	2.020(3)
Cu(1)-N(2)	2.156(3)	Cu(1)-O(2)	1.946(2)
Cu(1)-N(3)	1.947(2)		
O(2)-Cu(1)-N(1)	95.36(10)	N(3)-Cu(1)-N(2)	86.26(10)
O(2)-Cu(1)-N(2)	94.48(10)	N(4)-Cu(1)-N(2)	123.95(10)
O(2)-Cu(1)-N(3)	175.91(10)	N(3)-Cu(1)-N(1)	88.70(10)
O(2)-Cu(1)-N(4)	95.00(11)	N(4)-Cu(1)-N(1)	146.84(10)
N(3)-Cu(1)-N(4)	81.28(11)	N(2)-Cu(1)-N(1)	86.46(10)

acetonitrile (N(5)) and one perchlorate counterion (O(2)) (Fig. 8). As the cadmium ion possesses no stereochemical 15 preference, it can be reasonably assumed that in contrast to both L^3 and L^2, ligand L^1 does not naturally adopt a trigonal prismatic conformation.
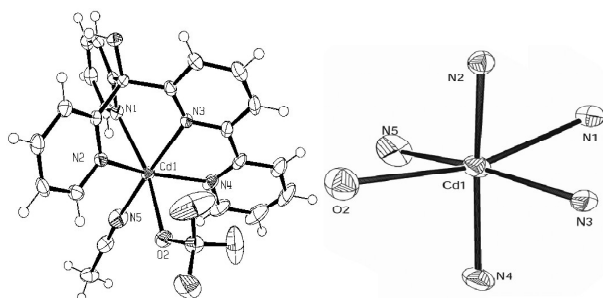

Fig. 8 A view of the core geometry of **7** showing the atom numbering. Displacement ellipsoids are shown at the 50% probability level.

20

The three mutually *trans* sets of donor atoms all form significantly less obtuse bond angles than the expected 180°; N(1)-Cd(1)-O2 (159.56(9)°), N(2)-Cd(1)-N(4) (149.32(10)°), 25 and N(3)-Cd(1)-N(5) (169.24(11)°). The narrow bite angle of the bipy unit (N(3)-Cd(1)-N(4) = 72.38(11)°) is also another source of distortion from the regular octahedron. The co-ordinative bond angles between pyridyl N-donors on the three pyridine rings lying closest to the methine bridge are 30 76.98(9)°, 78.28(9)° and 84.69(9)°, corresponding to the angles N(1)-Cd(1)-N(2), N(1)-Cd(1)-N(3) and N(2)-Cd(1)-N(3) respectively. These angles are all clearly more acute than the equivalent angles in the analogous nickel and copper complexes of L^1 (mean angles 86.59(11)° and 87.17(11)° 35 respectively). The larger radius of the second row cation causes it to lie further out from the plane (1.54109(18) Å) as defined by N(1), N(2) and N(3) (Fig. 9). The Ni and Cu cations have very similar radii and lie at an almost identical distance from this plane (1.2450(5) Å and 1.2407(4) Å 40 respectively).
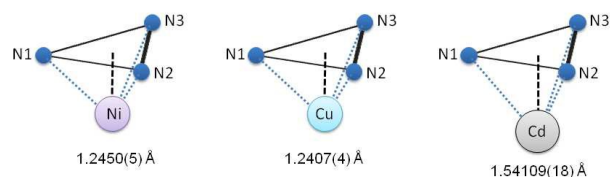

Fig. 9 The co-ordinative bond angles (*i.e.* N···M^{2+}···N) between the N-donors lying closest to the methine bridge are more acute for the cadmium complex (mean angle = 80.00(10)°) than the nickel and copper complexes (mean angles 86.59(11)° and 87.17(11)° respectively).

45 The mean average angle between the three donor atoms lying furthest from the methine bridge is 88.97(12)°, leading to a slightly truncated geometry surrounding the Cd^{II} centre. An example of a similar six co-ordinate octahedral structure is the compound bis(perchlorate-O)-tetrapyridine-cadmium(II).[30] 50 Here, the pyridyl N-Cd^{II} bond lengths range from 2.289(5) Å to 2.347(4) Å, and the perchlorate O-Cd^{II} bond length is 2.381(6) Å. These values are comparable to those in compound **7**.

Table 5 Significant Bond lengths (Å) and Angles (°) for 55 [Cd^{II}(L^1)(ClO$_4$)(CH$_3$CN)][ClO$_4$] (**7**)

Cd(1)-N(1)	2.350(3)	Cd(1)-N(4)	2.257(3)
Cd(1)-N(2)	2.284(3)	Cd(1)-N(5)	2.254(3)
Cd(1)-N(3)	2.284(3)	Cd(1)-O(2)	2.479(2)
N(5)-Cd(1)-N(4)	100.02(12)	N(2)-Cd(1)-N(1)	76.98(9)
N(5)-Cd(1)-N(2)	105.00(11)	N(3)-Cd(1)-N(1)	78.28(9)
N(4)-Cd(1)-N(2)	149.32(10)	N(5)-Cd(1)-O(2)	84.57(10)
N(5)-Cd(1)-N(3)	169.24(11)	N(4)-Cd(1)-O(2)	82.34(10)
N(4)-Cd(1)-N(3)	72.38(11)	N(2)-Cd(1)-O(2)	82.64(9)
N(2)-Cd(1)-N(3)	84.69(9)	N(3)-Cd(1)-O(2)	101.57(9)
N(5)-Cd(1)-N(1)	99.07(10)	N(1)-Cd(1)-O(2)	159.56(9)
N(4)-Cd(1)-N(1)	116.43(10)		

Table 6 Crystal structure data for complexes **8, 9, 10 and 14**

	[MnL^2(CH$_3$CN)]$^{2+}$ **8**	[FeL^2(CH$_3$CN)]$^{2+}$ **9**	[CoL^2(CH$_3$CN)]$^{2+}$ **10**	[CdL^2(CH$_3$CN)]$^{2+}$ **14**
M(1)-N(1)	2.293(2)	1.976(3)	2.172(3)/2.130(3)	2.350(3)
M(1)-N(2)	2.241(2)	1.927(3)	2.097(3)/2.102(3)	2.328(3)
M(1)-N(3)	2.262(3)	2.017(3)	2.135(4)/2.229(3)	2.315(3)
M(1)-N(4)	2.239(3)	1.907(3)	2.095(3)/2.112(3)	2.326(3)
M(1)-N(5)	2.263(3)	1.979(3)	2.217(3)/2.114(3)	2.327(3)
M(1)-N(6)	2.250(3)	1.953(3)	2.098(4)/2.118(4)	2.349(4)
N(1)-M(1)-N(2)	81.51(9)	91.06(14)	81.76(12)/87.46(13)	78.44(11)
N(1)-M(1)-N(3)	133.20(9)	168.76(13)	115.80(13)/153.67(12)	127.44(12)
N(1)-M(1)-N(4)	80.04(9)	84.31(13)	86.26(13)/79.37(12)	80.16(11)
N(1)-M(1)-N(5)	128.70(9)	101.03(13)	151.91(12)/114.17(13)	132.21(11)
N(1)-M(1)-N(6)	87.69(10)	89.84(13)	88.30(13)/89.20(12)	89.00(12)
N(2)-M(1)-N(3)	72.49(9)	80.33(14)	76.11(14)/74.02(12)	71.43(12)
N(2)-M(1)-N(4)	79.80(9)	89.14(13)	82.91(13)/84.01(13)	77.99(11)
N(2)-M(1)-N(5)	132.78(10)	163.30(14)	114.29(12)/146.74(13)	128.62(11)
N(2)-M(1)-N(6)	137.41(10)	95.21(13)	162.20(13)/108.36(13)	139.12(13)
N(3)-M(1)-N(4)	130.16(9)	102.63(14)	146.36(13)/116.11(12)	131.20(12)
N(3)-M(1)-N(5)	96.89(10)	88.91(14)	91.12(13)/90.95(13)	100.02(12)
N(3)-M(1)-N(6)	86.18(10)	83.81(14)	95.28(15)/79.40(12)	86.89(13)
N(4)-M(1)-N(5)	72.89(9)	80.74(14)	73.82(13)/76.17(13)	70.95(11)
N(4)-M(1)-N(6)	138.58(10)	172.79(14)	111.27(14)/162.90(14)	138.29(12)
N(5)-M(1)-N(6)	85.08(10)	96.30(13)	80.98(13)/97.40(13)	88.26(12)

^{a} Footnote text.

Crystal Structure of [Mn^{II}(L^2)(CH$_3$CN)][ClO$_4$]$_2$·(CH$_3$CN) (8)

The Mn^{II} complex of L^2 crystallises in the monoclinic space group P2$_1$/n with one complex within the asymmetric unit (Fig. 10a). The manganese is co-ordinated by all five pyridyl N-donors (N(1)-N(5)) of L^2 and a further N donor atom (N(6)) located on a solvent molecule of acetonitrile (Fig. 10b). This donor set is identical to the analogous Fe^{II}, Co^{II} and Cd^{II} complexes of L^2.

Fig. 10 a) Perspective view of the asymmetric unit of **8** showing the atom numbering. b) A view of the core geometry of **8** showing the atom numbering. Displacement ellipsoids are shown at the 50% probability

level.
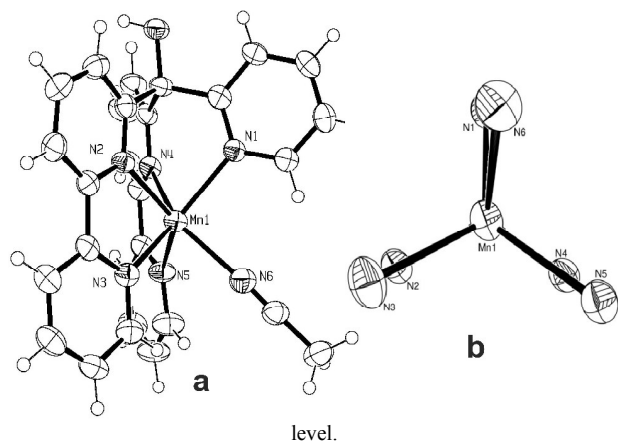
The co-ordinative bond lengths (Table 6) are well within the expected range, for example the similar compound [Mn^{II}(bpy)$_3$][ClO$_4$]$_2$ reveals pyridyl N-Mn^{II} bond distances ranging from 2.214(4) Å to 2.294(4) Å.[31] (*S*(TP) = 12.7, *S*(Oh) = 2.0) and [MnL^3][ClO$_4$]$_2$ has bond lengths ranging from 2.221(4) Å to 2.278(4) Å (*S*(TP) = 1.49, *S*(Oh) = 12.77).[11] In this instance the core geometry has more trigonal prismatic content than octahedral (*S*(TP) = 0.75, *S*(Oh) = 16.12), exhibiting a mean Bailar twist angle of 2.0°. The very slight increased TP character of **8** compared to [MnL^3][ClO$_4$]$_2$ relates to a truncated geometry being more strongly enforced in L^3.

The mean *s/h* ratio is 1.08 indicating a very slight compression relative to an ideal trigonal prism, which is clearly due to the narrow bite angle of the two bipyridyl groups. The mean N···N distances between the three donor atoms closest to the methine bridge are significantly shorter (2.915(3) Å) than those between the three distal N donors (3.170(3) Å), resulting in a truncated geometry around the metal centre. This generates a core geometry with pseudo-C$_{3v}$ symmetry, in contrast to the D$_{3h}$ symmetry observed in regular trigonal prisms. The Mn^{II} cation does not have any stereochemical preference in its high-spin configuration, thus, L^2 may be considered to be predisposed to yielding trigonal prismatic coordination spheres.

Crystal Structure of [Fe^{II}(L^2)(CH$_3$CN)][ClO$_4$]$_2$·(CH$_3$CN) (9)

The Fe^{II} complex of L^2 crystallises in the triclinic space group P-1 with one complex within the asymmetric unit. The donor set surrounding the Fe^{II} cation is identical to the analogous Mn^{II} complex (see ESI Figure 1), however, the co-ordination geometry in this instance is predominantly octahedral (*S*(Oh) = 1.35, *S*(TP) = 10.30). This indicates that the strong stereochemical preference of the d^6 ion (when low-spin) allows L^2 to adopt an octahedral conformation. The Bailar twist angle in this instance is 45.8° which is the largest for

Dalton Transactions Accepted Manuscript

Table 7 CShM results: Six-coordinate structures of L^1 and L^2

Structure	HP	PPY	OC	TPR	JPPY
L^1-Ni (**4**)	27.69	21.92	1.45	10.67	25.48
L^1-Cd (**7**)	27.38	18.76	3.95	7.15	22.22
L^2-Mn(CH$_3$CN) (**8**)	31.21	13.39	16.12	0.75	17.43
L^2-(Br)Mn *	34.73	17.30	9.17	3.16	20.51
L^2-Fe(CH$_3$CN) (**9**)	30.74	22.66	1.35	10.30	26.05
L^2-(Br)Fe *	34.28	17.27	7.00	4.35	21.00
L^2-Co(CH$_3$CN) (**10**)	32.02	17.34	5.76	4.36	20.69
L^2-Co(CH$_3$CN) (**10**)^a	33.11	17.89	5.96	3.96	21.43
L^2-(Br)Co *	32.18	17.62	5.47	5.95	20.56
L^2-Ni(Br) (**11**)	31.10	19.32	3.75	8.13	22.11
L^2-Ni(Br) *	31.91	19.60	3.86	7.73	22.71
L^2-Cd (**14**)	31.05	12.98	16.40	1.09	16.81

^{a} Compounds **10** contains two crystallographically independent complexes present within the asymmetric unit. HP (hexagon D$_{6h}$); PPY (pentagonal pyramid C$_{5v}$); OC (octahedron O$_h$); TP (trigonal prism D$_{3h}$); JPPY (Johnson pentagonal pyramid J2 C$_{5v}$).

this series of compounds.

The co-ordinative bond lengths (Table 6) are virtually identical to those found in the similar compound [Fe^{II}(bipy)$_3$][ClO$_4$]$_2$ which range from 1.953(3) Å to 1.972(3)Å.[32] The bipyridine groups are considerably bent in order to satisfy the stereochemical requirements of the metal; the dihedral angle between N(2)/C(7)-C(11) and N(3)/C(12)-C(16) is 28.2(3)° and the dihedral angle between N(4)/C(17)-C(21) and N(5)/C(22)-C(26) is 13.8(2)°. The bond angles between the three sets of mutually *trans* donor atoms, N(1)-Fe(1)-N(3), N(2)-Fe(1)-N(5) and N(4)-Fe(1)-N(6) are 168.95(14)°, 163.44(15)° and 172.90(15)° respectively, which all deviate significantly from the ideal 180°. Again, the steric restrictions imposed by the central carbon bridge upon the immediately adjacent pyridines lead to truncation, *i.e.* the mean N···N distance between the proximal N(1), N(2) and N(4) set of atoms (2.696(3) Å) is slightly shorter than between the more distal N(3), N(5) and N(6) set of atoms (2.791(3) Å).

Crystal Structure of [Co^{II}(L^2)(CH$_3$CN)][ClO$_4$]$_2$·0.5(H$_2$O) (10)

The Co^{II} complex of L^2 crystallises in the monoclinic space group P2$_1$/C with two symmetrically unrelated complexes within the asymmetric unit. (see ESI Figure 2) The donor atom sets surrounding the metal centres are consistent with Mn^{II}, Fe^{II} and Cd^{II} analogues and in all instances the geometry surrounding the metal centre has slightly more trigonal prismatic character than octahedral (S(TP) for the independent complexes = 4.36 and 3.96, S(Oh) = 5.76 and 5.96). This indicates a higher degree of TP character in **10** than in the analogous Fe^{II} and Ni^{II} complexes of L^2, which is most likely a consequence of the lower octahedral preference of the Co^{II} ion. The mean Bailar twist angles of complexes 1 and 2 are 26.60° and 27.70°, furthermore the mean s/h ratio in both instances is 1.12 indicating significant compression. These values serve to highlight the extent of the departure from an ideal trigonal prism. The co-ordinative bond lengths are similar to those within the complex [Co^{II}(bpy)$_3$][ClO$_4$]$_2$, which range from 2.119(2) to 2.136(2) Å.[33] The mean N···N distance between the three donor atoms closest to the methine bridge (2.820(3) Å) is significantly shorter than the mean distance between the three distal N donors (3.016(4) Å), resulting in a truncated geometry with pseudo-C$_{3v}$ symmetry.

Crystal Structure of [Cd^{II}(L^2)(CH$_3$CN)][ClO$_4$]$_2$·(CH$_3$CN) (14) The Cd^{II} complex of L^2 crystallises in the monoclinic space group P2$_1$/n and contains one complex within the asymmetric unit. The Cd^{II} ion is co-ordinated in an identical fashion to the analogous Mn^{II}, Fe^{II} and Co^{II} complexes, *i.e.* by all five pyridyl N-donors (N(1)-N(5)) and an N donor (N(6)) located on a solvent acetonitrile molecule (see ESI Figure 3). The co-ordination geometry surrounding the metal is clearly trigonal prismatic, confirmed by the shape mapping results (S(TP) = 1.09 and S(Oh) = 16.40). This is also reflected by the small Bailar twist angle (1.883°). There are, however, some minor distortions from an ideal TP environment. For example, the mean s/h ratio is 1.09 which indicates a slight compression along one axis. Furthermore, the mean N···N distance between the N-donors lying closest to the methine bridge is 2.964(4) Å, whilst the mean distance between three furthest lying N-donors (3.337(4) Å) is significantly larger, indicating truncation of the trigonal prism leading to pseudo-C$_{3v}$ symmetry. The co-ordinative bond lengths (Table 6) span a very similar range compared to those of the similar compound [Cd^{II}(bpy)$_3$][ClO$_4$]$_2$ which range between 2.308(5) Å and 2.355(5) Å in an unconstrained octahedral environment.[34]

Structural Overview and Continuous Shape Mapping

Typically, the observed metal geometry is an optimisation of the highest ligand field stabilisation energy (LFSE) against the lowest possible steric strain energy. Although the LFSE varies with d electron configuration, in most cases, octahedral geometries have higher LFSE than the analogous trigonal prismatic geometry. Indeed, typically for six monodentate ligands, the lowest steric interactions are observed for an octahedral arrangement compared to the trigonal prismatic. Thus, the isolation of trigonal complexes for late transition metal complexes will primarily be driven by the design of polydentate ligands which sterically prefer a trigonal prismatic geometry.

Dalton Transactions Accepted Manuscript

Table 8 The mean average Bailar twist angles for complexes **4, 7-11** and **14** amongst other pertinent data.

Compound	Bailar twist angle, φ, °	s/h	Mean bond M···N length, Å	Dihedral angle between trigonal faces, °	Effective ionic radius of the metal ion (pm)[35]
L[1]-Ni (**4**)	33.23	1.13	2.081	5.58(16)	69
L[1]-Cd (**7**)	36.87	1.08	2.319	11.10(16)	95
L[2]-Mn (**8**)	2.00	1.08	2.714	11.00(17)	67
L[2]-Fe (**9**)	45.8	1.19	1.959	1.4(2)	61(ls), 78(hs)
L[2]-Co (**10**)	26.6	1.12	2.135	5.5(2)	65(ls), 74.5(hs)
L[2]-Co (**10**)[a]	27.7	1.12	2.135	3.85(19)	65(ls), 74.5(hs)
L[2]-Ni (**11**)	37.6	1.16	2.170	5.6(2)	69
L[2]-Cd (**14**)	1.87	1.09	2.331	12.99(19)	95

Hexadentate L[3] has all donor atoms ideally arranged for TP co-ordination, but L[1] and L[2] have fewer didentate bipyridyl arms than L[3], and the steric strain required to twist the ligand, to produce an octahedral geometry is decreased. Therefore, one expects a reducing capacity for enforcing trigonal prismatic co-ordination modes, from L[3] to L[1]. From the observed results we can conclude:

(i) the complexes of Cd[II], a d[10] cation, will have no stereoelectronic preferences and their geometry will be largely driven by steric factors. The cadmium complex of L[1] has continuous shape measures of S(TP) = 7.15 and S(Oct) = 3.95, confirming a predominantly octahedral co-ordination sphere. In contrast, the Cd[II] centre of the corresponding L[2] complex, shows a strong preference for trigonal prismatic geometry (S(TP) = 1.09). Similarly, the isoelectronic Mn(II) complex of L[2] is also trigonal prismatic (S(TP) = 0.75). These results suggest that for d[10] complexes, steric interactions of the ternary acetonitrile ligands with L[1] are significant enough to produce more octahedral character.
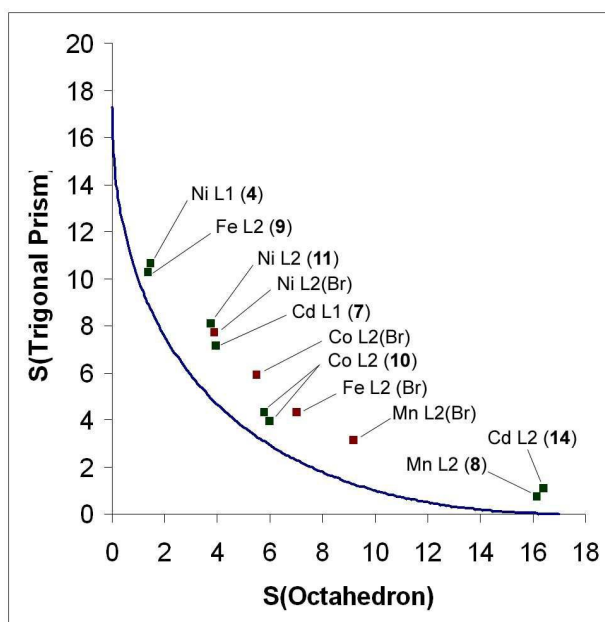

Fig. 11 Octahedron – Trigonal Prism shape map showing the Bailar pathway (continuous line) and the experimental data for L[1] and L[2] in this work(green squares) and from previous studies (brown squares)

(ii) There is reducing TP-character of complexes from the ligands progressing from L[3] to L[1]; it is interesting to note that while L[3] maintains near-TP configurations in the presence of metal ions with strong octahedral preferences, L[2] now distorts towards predominantly octahedral co-ordination spheres. The octahedral character in the complexes of L[2] is greatest for Fe[II]. Unlike the tris bipyridyl ligand, L[3], where the order of O_h character is Ni[II] > Co[II] > Fe[II], for L[2] now Fe[II] has more octahedral character than Co[II]. This could be explained by the formation of low spin octahedral Fe[II] complexes with L[2], which is confirmed by the short Fe-N distances observed.

(iii) A representation of the calculated values in a shape map (Fig. 11; Table 7) illustrates that all structures are close to the Bailar path for the interconversion of the trigonal prism and the octahedron. It is likely that any minor deviations from this path are due to the constrained geometry of the tetra- and pentadentate tripodal ligand frameworks.

(iv) On considering the shape values of previously reported complexes, [ML[2]Br][Br][12,13] it becomes clear that the nature of the ternary ligand may have a notable effect on the observed geometry for some complexes. Most prominent is the different geometries observed with the iron complexes. It is difficult to determine if the cause of the variance is electronic or steric, but one expects both ligands to be weak donors. However, bromide is much more sterically demanding than CH₃CN. While all the metal bromide complexes distort to give approximately similar structures, the Fe(II) acetonitrile complex is able to form the electronically favoured octahedral complex.

(v) The copper compound of L[1], **5**, differs from the other compounds by adopting a five co-ordinate geometry which lies almost exactly halfway between trigonal bipyramidal and square pyramidal (ESI Fig.4, Table 9; (S(TBPY) = 3.35 and S(SPY) = 3.38).

Table 9 Continuous Shape Mapping Results – Five Co-ordinate Structures

Structure	VOC	TBPY	SPY	JSPY	JTBP
L[1]-Cu (**5**)	3.91	3.35	3.38	3.91	6.65

[a] VOC (vacant octahedron C₄ᵥ); TBPY (trigonal bipyramid D₃ₕ); SPY (spherical square pyramid C₄ᵥ); JSPY (Johnson square pyramid J1); JTBP (Johnson trigonal bipyramid J12)

Conclusions

In summary, these related ligands display a notable variation in their geometric preferences when coordinated to transition metals. While ligand, L^1, predefines four of the six donors in a trigonal prismatic co-ordination sphere, does not actually enforce the geometry and the ligand has sufficient flexibility to form the electronically favoured octahedral geometry. While this may not be surprising in the context of metal ions where the LFSE leads to a strong preferance for O_h geometry, O_h structures were still observed in ions with no LSFE. Similarly, L^2, defines five of the six trigonal prismatic donor sites. In this case, the geometry observed is heavily influenced by the geometric preference of the metal centre. Finally, it appears that only L^3, which predefines all six donor positions, is able to yield trigonal prismatic complexes irrespective the of the transition ion. These results suggest studies aimed at designing four or five co-ordinate ligands enforcing TP geometry in metals where the LSFE favours O_h geometry will be challenging.

Notes and references

a School of Chemistry,Cardiff University, Cardiff, South Glamorgan. Fax: 29 2087 4030; Tel:29 20874077; E-mail:amorosoaj@cf.ac.uk

† Electronic Supplementary Information (ESI) available: [details of any supplementary information available should be included here]. Crystallographic data in CIF format CCDC 1470082-1470089.
See DOI: 10.1039/b000000x/

1. R. Eisenberg, J.A. Ibers, *J. Am. Chem. Soc.*, 1965, **87**, 3776.
2. R. Eisenberg, J.A. Ibers, *Inorg. Chem.*, 1966, **5**, 411.
3. A.E. Smith, G.N. Schrauzer, V.P. Mayweg, W. Heinrich, *J. Am. Chem. Soc.*, 1965, **87**, 5798; R. Eisenberg, E.I. Stiefel, R.C. Rosenberg, H.B. Gray, *J. Am. Chem. Soc.*, 1966, **88**, 2874.
4. D.L. Kepert, *Prog. Inorg. Chem.*, 1977,**23**, 1.
5. R. van Gorkum, F. Buda, H. Kooijman, A.L. Spek, E. Bouwman, J. Reedijk, *Eur. J. Inorg. Chem.*, 2005, 2255 and references therein.
6. R.A.D. Wentworth, W.O. Gillum, R. F. Childers, *Inorg. Chem.*, 1970, **9**, 1825-1832.
7. W.O. Gillum, J.C. Huffman, W.E. Streib, R.A.D. Wentworth, *Chem. Commun.*, 1969, 843.
8. D.R. Boston, N.J. Rose, *J. Am. Chem. Soc.*, 1968, **90**, 6859.
9. J. E. Parks, B.E. Wagner, R.H. Holm, *Inorg. Chem.*, 1971, **10**, 2472; J. E. Parks, B.E. Wagner, R.H. Holm, *J. Am. Chem. Soc.*, 1970, **92**, 3500.
10. T.B. Karpishin, T.D.P. Stack, K.N. Raymond, *J. Am. Chem. Soc.*, 1993, **115**, 182.
11. J. C. Knight, S. Alvarez, A.J. Amoroso, P.G. Edwards, N. Singh, *Dalton Trans.* 2010, **39**, 3870.
12. M. Guttentag, A. Rodenberg, C. Bachmann, A. Senn, P. Hamm, R. Alberto, *Dalton Trans.*, 2013, **42**, 334.
13. C. Bachmann, M. Guttentag, B. Spingler, R. Alberto, *Inorg. Chem.*, *2013*, **52**, 6055-6061.
14. S. Alvarez, D. Avnir, M. Llunell, M. Pinsky, *New J. Chem.*, 2002, **26**, 996-1009; S. Alvarez, D. Avnir, P. Alemany, *Chem. Soc. Rev.*, 2005, **34**, 313-326; S. Alvarez, D. Avnir, P. Alemany, D. Casanova, M. Llunell, J. Cirera, *Coord. Chem. Rev.*, 2005, **249**, 1693-1708; S. Alvarez, D. Avnir, M. Pinsky, M. Llunell, *Cryst. Engineer.* 2001, **4**, 179-200; M. Pinsky, D. Avnir, *Inorg. Chem.*, 1998, **37**, 5575-5582; M. Pinsky, K.B. Lipkowitz, D. Avnir, *J. Math. Chem.*, *2001*, **30**, 109-120.
15. N. Singh, PhD Thesis, Cardiff University, 2008.
16. J.C. Knight, PhD Thesis, Cardiff University 2010.
17. A.B.P. Lever, *Coord. Chem. Rev.*, 1968, **3**, 119.
18. B.F. Little, G.J. Long, *Inorg. Chem.*, 1978, **17**, 3401.
19. G.M. Bancroft, K.D. Butler, *J. Chem. Soc., Dalton Trans.*, 1972, 1209.
20. W.C. Jones, W.E. Ball, *J. Chem. Soc. (A)*, 1968, 1849.
21. B.J. Hathaway, D.E. Billing, *Coord. Chem. Rev.*, 1970, **5**, 143.
22. W. Fitzgerald, B. Murphy, S. Tyagi, B. Walsh, B.J. Hathaway, *J. Chem. Soc., Dalton Trans.*, 1981, 2271.
23. R.H. Blessing, *Acta Crystallogr.*, 1995, **A51**, 33.
24. P. van der Sluis and A. L. Spek, *Acta Cryst.*, 1990, **A46**, 194.
25. D.T. Cromer, and J. T. Waber, International Tables for Crystallography; The Kynoch Press: Birmingham, 1974.
26. G. M. Sheldrick, *Acta Cryst.*, 2008, **A64**, 112.
27. L.J Farrugia, *J. Appl. Crystallogr.*, 1997, **30**, 565.
28. J.M. Zadrozny,D.E Freedman, D.M. Jenkins, T.D. Harris, A.T. Iavarone, C. Mathoniere, R. Clerac, J.R. Long *Inorg.Chem.* 2010, **49**, 8886.
29. G. Murphy, C. Murphy, B. Murphy, B.J. Hathaway, *J. Chem. Soc., Dalton Trans.*, 1997, 2653.
30. C.-F. Ding, M. Zhu, X.-M. Li, S.-S. Zhang, H. Xu, P.-K. Ouyang, *Asian J. Chem.*, 2006, **18**, 1685. CCDC deposition no. 646794.
31. X.-M. Chen, R.-Q. Wang, Z.-T. Xu, *Acta Crystallogr.*, 1995, **C51**, 820.
32. S. R. Batten, K. S. Murray, N. J. Sinclair, *Acta Crystallogr.*, 2000, **C56**, e320.
33. J.-C. Yao, L.-F. Ma, F.-J. Yao, *Z. Kristallogr.-New Cryst. Struct*, 2005, **220**, 483. CCDC deposition no. 240261.
34. M. Chaudhury, E.R.T. Tiekink, D. Mandal, N. Kundu, *Appl. Organomet. Chem.*, 2005, **19**, 1268. CCDC deposition no. 275094.
35. R.D. Shannon, *Acta Crystallogr.*, 1976, **A32**, 751-767.

Dalton Transactions Accepted Manuscript

Graphical Abstract

The coordination chemistry of two tripodal frameworks, mono(2,2'-bipyrid-6-yl)bis(2-pyridyl)methanol (L^1) and bis(2,2'-bipyrid-6-yl)mono(2-pyridyl)methanol (L^2) are contrasted to the related ligand, tris(2,2'-bipyrid-6-yl)methanol (L^3). L^1, and to a lesser degree L^2, overcome steric strain to produce octahedral complexes compared to the stronger trigonal prismatic preference observed in the complexes of L^3.